Supporting Information

Optical metasurfaces for generation and superposition of optical ring vortex beams

Jin Han, Yuttana Intaravanne, Aning Ma, Ruoxing Wang, Songtao Li, Zhancheng Li, Shuqi Chen, Jensen Li, Xianzhong Chen*

Supplementary Section 1. Nanofabrication procedure of the reflective metasurface.

In order to fabricate the designed metasurface, the standard electron-beam lithography (EBL) and lift-off process are used. First, a gold layer (150 nm) at the bottom and a SiO_2 spacer (85nm) on the top are deposited onto a silicon substrate by using an electron beam evaporator. Then, the positive polymethyl methacrylate (PMMA) resist film is spin coated onto the SiO_2 spacer layer and baked at 180 °C for 5 minutes. After that, the nanostructures are defined on the PMMA film by EBL (Raith PIONEER), a 30 nm gold film is deposited on the sample via electron beam evaporate. Finally, the metasurfaces (see Figure S1) are ready for characterization after the lift-off process in the acetone.

Supplementary Section 2. Generation of incident light with various polarization states

Any arbitrary complete polarization state can be decomposed into the LCP and RCP with various components. Therefore, the superposition of ring OAM beams can be continuously controlled by changing the polarization state of the incident light.

Different polarization states of incident light are obtained by rotating the angle between the transmission axis of a linear polarizer and the fast axis of a quarter wave plate (QWP). Suppose the angle between the fast axis of QWP with respect to the x-axis is α, the angle between the transmission axis of a linear polarizer with respect to the x-axis is β, The Jones matrix of the QWP and the linear polarizer are $e^{-i\frac{\pi}{4}}\begin{bmatrix} \cos^2\alpha + i\sin^2\alpha & (1-i)\sin\alpha\cos\alpha \\ (1-i)\sin\alpha\cos\alpha & \sin^2\alpha + i\cos^2\alpha \end{bmatrix}$ and $\begin{bmatrix} \cos\beta \\ \sin\beta \end{bmatrix}$, respectively.

The Jones vector of the light beam after passing through the polarizer and the QWP is governed by the following relation:

$$e^{-i\frac{\pi}{4}}\begin{bmatrix} \cos^2\alpha + i\sin^2\alpha & (1-i)\sin\alpha\cos\alpha \\ (1-i)\sin\alpha\cos\alpha & \sin^2\alpha + i\cos^2\alpha \end{bmatrix}\begin{bmatrix} \cos\beta \\ \sin\beta \end{bmatrix} = a\begin{bmatrix} 1 \\ -i \end{bmatrix} + b\begin{bmatrix} 1 \\ i \end{bmatrix}$$

Wher $a = \frac{\sqrt{2}}{4}\left(\sin 2\alpha\cos\beta + \cos\beta - \cos 2\alpha\sin\beta + i(-\cos 2\alpha\cos\beta - \sin 2\alpha\sin\beta + \sin\beta)\right)$ and

$b = \frac{\sqrt{2}}{4}\left(-\sin 2\alpha\cos\beta + \cos\beta + \cos 2\alpha\sin\beta + i(-\cos 2\alpha\cos\beta - \sin 2\alpha\sin\beta - \sin\beta)\right)$ are the components of LCP and RCP light, respectively.

Supplementary Section 3. The results of different polarization states of the incident light at 650 nm illumination upon samples

Figure S2 shows the experimentally measured results versus different polarization states of the incident light at 650 nm. The superposition doesn't exist for pure circular polarizations (LCP or RCP), but it occurs for elliptical polarizations.

Supplementary Section 4. The experimental and the simulation results for the measurement of major axis of the polarization state without analyser.

Supplementary Section 5: The experimental results for the superpositions of ring OAM beams at other wavelengths.

Figure S4 shows the experimental results at different wavelengths. The green, yellow and red rings correspond to the incident light at the wavelengths of 532nm, 581nm and 650nm, respectively. The incident light is linearly polarized along the vertical direction. The screen is perpendicular to the propagation of the incident light, thus the center of each ring light beam on one side is not perpendicular to the screen, leading to the image distortion.

Supplementary Section 6: The simulation results for the superpositions of two ring OAM beams with different combinations of diameters.

The simulated normalized intensity distributions at the screen plane are calculated based on the Fresnel–Kirchhoff diffraction integral. In our simulation, the existence of dim ring within the designed inner ring is due to the weak coupling between inner and outer rings. Fig.S5 shows the simulation results for the superpositions of two ring OAM beams with different combinations of diameters, which are determined by the axicon periods. The axicon period d_2 for the outer ring is chosen to be $4\ \mu m$, while the axicon periods d_1 for the inner rings are 6 μm and 12 μm, respectively. When the ring radius difference between the inner and outer rings become larger, the coupling is negligible and the dim ring disappears (shown in Fig.S5 (b)).

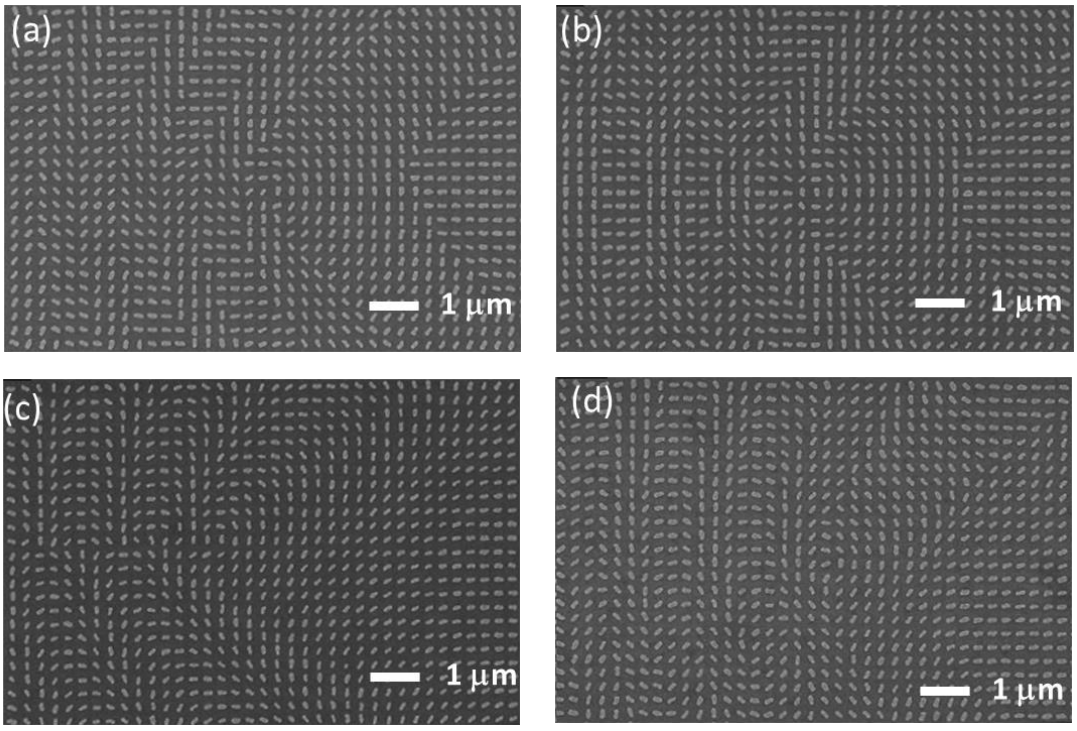

Fig. S1 The scanning electron microscope (SEM) images of the fabricated metasurfaces. Metasurfaces for the realization of superpositions of ring OAM beams with (a) $|L, \ell_1 = 2\rangle$ and $|R, \ell_2 = -2\rangle$, (b) $|L, \ell_1 = 1\rangle$ and $|R, \ell_2 = -2\rangle$, (c) $|L, \ell_1 = 1\rangle$ and $|L, \ell_2 = 2\rangle$, (d) $|L, \ell_1 = 1\rangle$, $|R, \ell_2 = -1\rangle$ for inner ring and $|L, \ell_3 = 1\rangle$, $|L, \ell_4 = 3\rangle$ for the outer ring. These metasurfaces have a dimension of 300 μm×300 μm and each pixel has a dimension of 300 nm×300 nm.

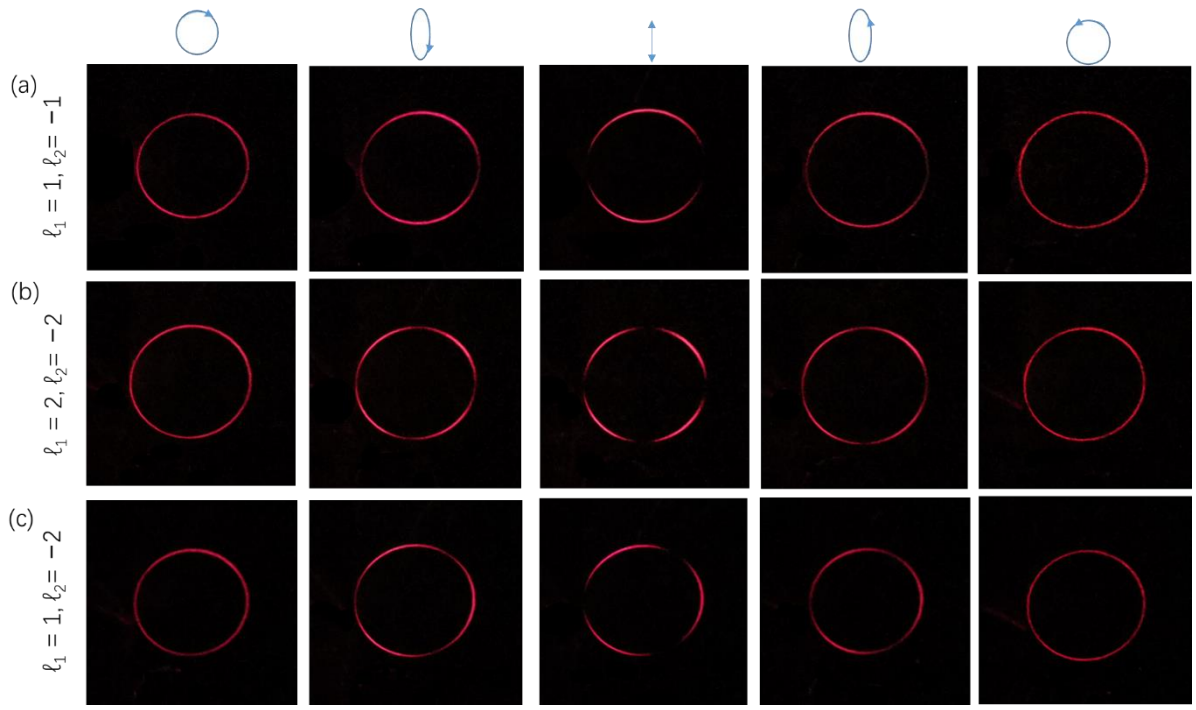

Fig. S2 Experimentally measured results versus different polarization states of the incident light at 650 nm upon samples. (a) $|L, \ell_1 = 1\rangle$ and $|R, \ell_2 = -1\rangle$, (b) $|L, \ell_1 = 2\rangle$ and $|R, \ell_2 = -2\rangle$, (c) $|L, \ell_1 = 1\rangle$ and $|R, \ell_2 = -2\rangle$, respectively.

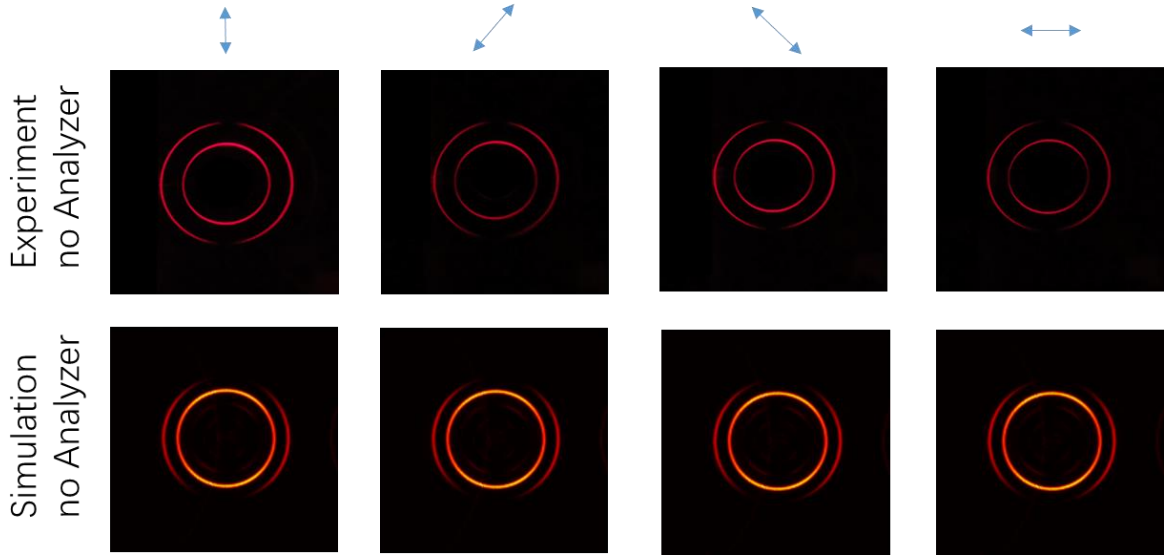

Fig. S3 The experimental and the simulation results for the measurement of major axis of the polarization state without the analyzer. The main axis of the incident LP is along 90 degree, 45 degree, -45 degree and 0 degree, respectively.

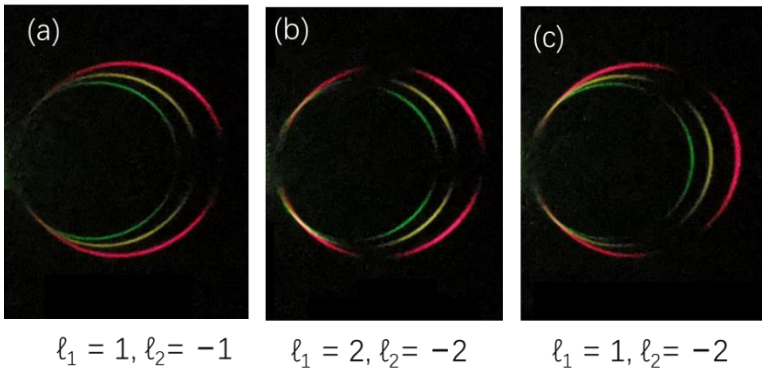

Fig. S4. Experimental results for the superpositions of ring OAM beams with (a) $|L, \ell_1 = 1\rangle$ and $|R, \ell_2 = -1\rangle$, (b) $|L, \ell_1 = 2\rangle$ and $|R, \ell_2 = -2\rangle$, (c) $|L, \ell_1 = 1\rangle$ and $|R, \ell_2 = -2\rangle$, respectively at other wavelengths.

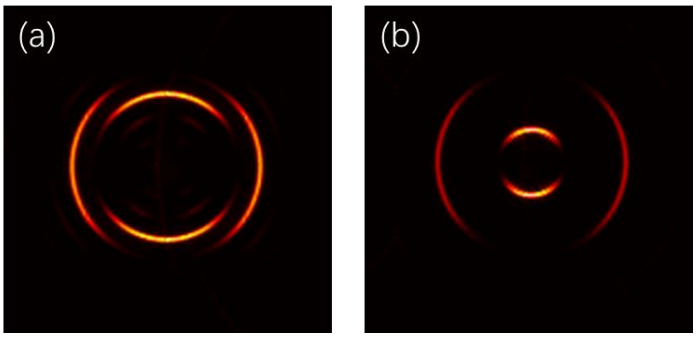

Fig. S5. Simulation results for the superpositions of two ring OAM beams with the superposition of $|L,\ell_1=1\rangle$ and $|R,\ell_2=-1\rangle$ for the inner ring and that of $|L,\ell_3=1\rangle$ and $|L,\ell_4=3\rangle$ for the outer ring. The axicon period for the outer ring is $d_2=4\ \mu m$, while the axicon periods for the inner ring are (a)$d_1=6\ \mu m$ and (b) $d_1=12\ \mu m$, respectively.

Supplementary Section 7: Influence of off-axis angle on the image quality

The off-axis design is used to simultaneously realize the superposition of OAM beams and remove the non-converted part. Fig.S6 shows the simulation results of ring OAM beams at different off-axis

angles. In our design, the off-axis angle (deflection angle) is 12.4° （$\Delta\phi_{off}=\pi/5$） at the wavelength of 650 nm. There is no image distortion in our design. However, the image distortion (acceptable) along the horizontal direction appears when the deflection angle is 15.7° ($\Delta\phi_{off}=\pi/3$). The image distortion becomes more and more serious at larger deflection angles. For example, the image distortion is much worse at 32.8° （$\Delta\phi_{off}=\pi/2$）. This is easy to understand since the paraxial approximation doesn't work any more. From the simulation results, we can see that the maximum deflection angle in our design is around 15°. The off-axis angle is calculated based on the equation $\sin\theta_{off}=\frac{\lambda_0}{2\Lambda}\frac{\Delta f_{off}}{\Delta x}$, where λ_0 is the wavelength of incident light, Δx is the period of nanorod along x-direction.

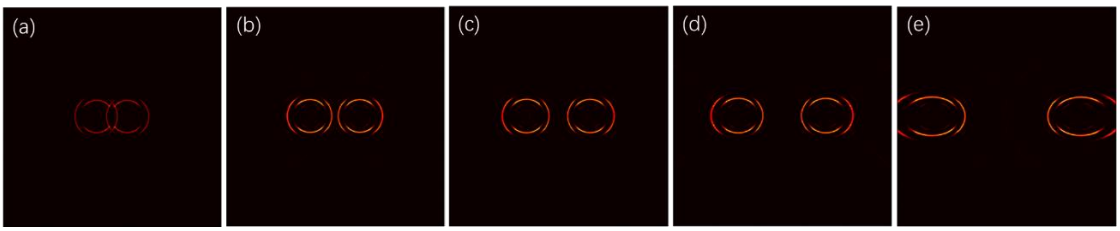

Fig. S6 Simulation results of ring OAM beams at different off-axis angles at 650 nm. The phase difference between neighboring pixels to generate a phase gradient along the horizontal (x-) direction are (a) $\Delta\phi_{off}=\pi/8$, (b) $\Delta\phi_{off}=\pi/5$, (c) $\Delta\phi_{off}=\pi/4$, (d) $\Delta\phi_{off}=\pi/3$, (e) $\Delta\phi_{off}=\pi/2$, corresponding to the off-axis angle 7.8°, 12.4°, 15.7°, 21.2° and 32.8°, respectively. The axicon period for the outer ring and inner ring are 4 μm and 6 μm, respectively.